IEEE Access
Multidisciplinary | Rapid Review | Open Access Journal

Received 17 April 2024, accepted 17 May 2024, date of publication 24 May 2024, date of current version 3 June 2024.

Digital Object Identifier 10.1109/ACCESS.2024.3405382

RESEARCH ARTICLE

Carrier Lifetime Dependence on Temperature and Proton Irradiation in 4H-SiC Device: An Experimental Law

GIOVANNA SOZZI[1], (Senior Member, IEEE), SERGIO SAPIENZA[2], GIOVANNI CHIORBOLI[1], LASSE VINES[3], ANDERS HALLÉN[4], AND ROBERTA NIPOTI[2]

[1]Department of Engineering and Architecture, Università di Parma, 43124 Parma, Italy
[2]CNR-IMM of Bologna, 40129 Bologna, Italy
[3]Department of Physics, Centre for Materials Science and Nanotechnology, University of Oslo, 0316 Oslo, Norway
[4]KTH Royal Institute of Technology, School of EECS, Kista, 164 40 Stockholm, Sweden

Corresponding author: Giovanna Sozzi (giovanna.sozzi@unipr.it)

ABSTRACT The study focuses on analysing the high-level carrier lifetime (τ_{HL}) in 4H silicon carbide (4H-SiC) PiN diodes under varying temperatures and proton implantation doses. The objective is to identify an empirical law applicable in technology computer-aided design (TCAD) modelling for SiC devices, describing the dependence of carrier lifetime on temperature to gain insights into how irradiation dose may influence the τ_{HL}. We electrically characterize diodes of different diameters subjected to different proton irradiation doses and examine the variations in current-voltage (I-V) and ideality factor (n) curves under various irradiation conditions. The effects of proton irradiation on the epitaxial layer are analysed through capacitance-voltage (C-V) measurements. We correlate the observed effects on I-V, n, and C-V curves to the hypothesis of formation of acceptor-type defects related to carbon vacancies, specifically the $Z_{1/2}$ defects generated during the irradiation process. The impact of irradiation on carrier lifetime is investigated by measuring τ_{HL} using the open circuit voltage decay (OCVD) technique at different temperatures on diodes exposed to various H^+ irradiation doses with constant ion energy. This investigation reveals the presence of a proportional relationship between $1/\tau_{HL}$ and the dose of irradiated protons: the proportionality coefficient, referred to as the damage coefficient (K_T), exhibits an Arrhenius-type dependence on temperature. OCVD-measured lifetime on the various diodes demonstrates a power-law dependence of lifetime on temperature. The exponent of this dependence varies with the irradiation dose, notably showing an increase in temperature dependence at the highest H^+ ion dose. This suggests a threshold-like dependence on H^+ irradiation dose in the τ_{HL}-temperature relationship.

INDEX TERMS Bipolar device, carrier lifetime, capacitance-voltage (C-V) measurements, damage coefficient, diode, OCVD, PiN, proton irradiation, 4H-SiC.

I. INTRODUCTION

Over the past two decades, silicon carbide (SiC) has garnered significant interest in power electronics applications. This surge in attention stems from its exceptional characteristics: a wide energy gap, remarkable thermal conductivity, and a high critical electric field [1]. These properties render SiC power devices exceedingly advantageous for high-voltage and high-power applications [2], [3]. In addition, being an indirect bandgap semiconductor, SiC potentially exhibits carrier lifetimes longer than direct semiconductors.

Accurate control of carrier lifetime and a thorough understanding of the injected carrier profile during on-state operation are crucial for optimizing bipolar devices, such as

The associate editor coordinating the review of this manuscript and approving it for publication was Marcelo Antonio Pavanello.

PiN diodes, IGBTs, BJTs, and thyristors. Efficiently utilizing conductivity modulation is key to mitigating power losses in these devices.

Extensive research has focused on understanding the origins of defects, minimizing their density in epitaxial layers [4], [5], and enhancing the device's on-state performance, thereby lowering the on-state resistance, R_{ON}.

Simultaneously, attempts have been made to locally reduce carrier lifetime within the same layer using irradiation techniques, with electrons or ions [6], [7], aiming to accelerate device switching, to finally achieve the optimal balance between continuous operation and switching mode [8], [9].

The performance of these devices, both during on-state and switching operations, relies heavily on the concentration and distribution of carriers and eventually the radiation induced deep-level defects within the voltage-blocking layer [1]. Consequently, gaining insights into the carrier lifetime within this region becomes crucial.

Another crucial aspect involves comprehending the temperature-dependent behavior of carrier lifetime; possessing these models is imperative for accurately simulating the performance of power devices under various operating conditions. Indeed, in contrast to the continuous theoretical modelling and characterization of materials like silicon spanning over five decades, the theoretical modelling of essential physical parameters necessary to describe the operation of SiC-based devices in numerous high-power applications through Technology Computer-Aided Design (TCAD), which enables predictive simulations, remains incomplete even in the modern context.

The aim of this study is to estimate the lifetimes of carriers in SiC before and after proton irradiation and extract a law that enables us to describe how these lifetimes vary with the temperature of the device and irradiation.

In fact, the device's operating temperature significantly influences carrier lifetime, potentially impacting multiple device properties. These include, but are not limited to, the device's R_{ON}, breakdown voltage, on-state and switching power losses, as well as diode reverse recovery and softness [1], [10].

II. DEVICE UNDER STUDY

The devices under examination are vertical cylindrical mesa PiN diodes, featuring anode sizes ranging between 200 and 700 μm. These diodes are fabricated on a homo-epitaxial 4° off (0001) 4H-SiC wafer and are contained within square chips measuring 2.5mm × 2.5mm [11].

The cross-sectional structure of the device in Fig. 1, including the layers' thicknesses, was determined through analysis using scanning electron microscopy (SEM) of a cross-sectioned specimen (refer to Figs. 9(a,b) in Appendix A for visual representations of this analysis). Further description of the sample is found in [11].

Some of the diodes were ion implanted at 7° tilt angle to avoid channeling effects with H^+ doses in the range $10^9 - 5 \times 10^{10}$ cm^{-2}, an energy of 800 keV and at RT at the ion implantation facility of UiO MiNaLab [12]. The projected length of the 800 keV H^+ implantation was 6.3 μm into the SiC layer, thus placing it firmly into the n-drift layer of the diode. Table 1 lists the measured samples along with their H^+ ion doses; each sample is a chip that contains diodes of different diameters of PN junction.

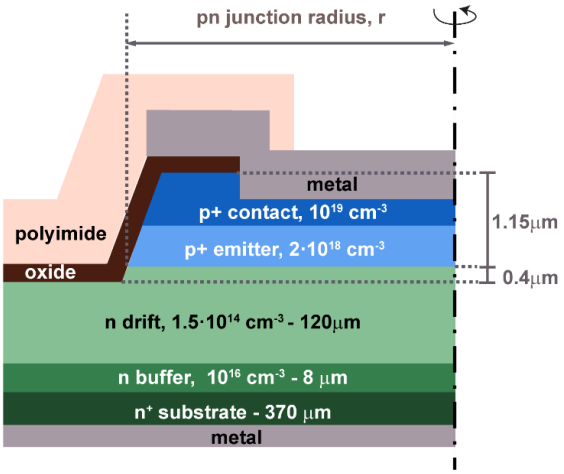

FIGURE 1. Half section of the vertical cylindrical diodes under study. The dash-dot line is the diode central axis of symmetry. The mesa etchings on the diode periphery and the anode come from SEM observations and it is about 0.4 μm deeper than the p-type emitter. The emitter's two layers' thicknesses result from the epitaxial growth process [11]. The metal is made of a thin Ti+W+Al layer topped by an approximately 0.5 μm thick Al film [11]. Not to scale.

TABLE 1. Samples list: the first digits SIC0386 are common to every label and identify the SiC wafer, while the last digit A, B, D, E, F, G, M, N, O, Q, S, and T identifies the chip. Apex "*" is used for TO mounted samples.

Sample label SIC0386	800 keV H^+ ion dose [cm^{-2}]
A*, B*, M, N, O	0
D*, Q	1×10^9
E*	5×10^9
F*, S	1×10^{10}
G*, T	5×10^{10}

The thick drift layer, measuring 120 μm, is designed for the fabrication of 10 kV diodes with suitable junction edge terminations. Nevertheless, the diodes under investigation were not subjected to high-voltage breakdown testing. Instead, the focus was solely on examining the impact of H^+ ion implantation on the anode side, as detailed below.

III. MEASUREMENTS SET-UPS

We conducted current-voltage (I-V) and capacitance-voltage (C-V) measurements on multiple diodes.

A. ON WAFER MEASUREMENTS

For the forward and reverse current-voltage characterization at the wafer level, we employed a setup including a temperature-controlled chuck and utilized Keithley

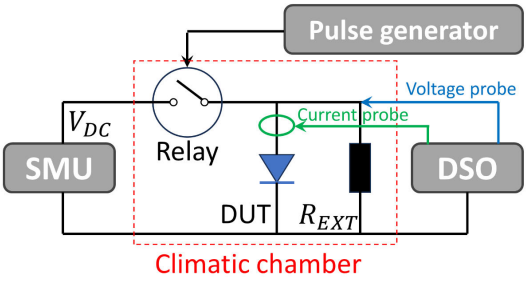

FIGURE 2. Experimental setup used for OCVD measurements: schematic of the OCVD electronic circuit.

instruments with multi-meters and a switching matrix. The measurements were carried out at a temperature of 298 K, and the set-up featured current and voltage compliances set at 100 mA and 100 V, respectively.

Additionally, we selected voltage steps, delay times, and hold-on times to ensure that the measured current floor fell within the low decade of 10^{-13}A. Even though we will discuss the results, we will only present the I-V characteristics of the measurements carried out on the packaged diodes.

B. MEASUREMENTS ON PACKAGED DEVICES

We also performed forward I-V, C-V, and OCVD (Open Circuit Voltage Decay) measurements on samples housed in TO-8 cases.

For the forward I-V measurements, we employed an HP4142B modular unit equipped with the HP 41429 DC Source/Monitor unit, setting the current and voltage compliances to 1 A and 200 V, respectively. Notably, we observed that the repeatability of these I-V curves remained within 1% for measured currents exceeding 1 nA.

For the C-V measurements, we used an HP4284A LCR meter at a frequency of 1 MHz. The oscillator level was set and maintained at 200 mV while conducting measurements across a bias range from −20 V to +2.4 V.

Fig.2 depicts a schematic of the OCVD measurement setup. The device under test (DUT) is a single PiN diode connected in parallel with a variable external resistor, R_{EXT}, spanning from 0 to 10 MΩ. R_{EXT} is needed to counteract the effect of parasitic capacitance during OCVD measurements, as outlined by Green [13].

The diode is initially biased in high injection using a DC voltage supply, V_{DC}. A pulse generator quickly disconnects the supply via a mercury relay (Fig. 2), which is closed by a 5 V, 1 ms pulse. The subsequent voltage decay, V(t), is recorded and the carrier lifetime is determined from the slope of the linear portion of the decay. A thorough explanation of the OCVD measurement can be found in [14].

During measurements, the TO-8 case is maintained within a Climate Chamber at a specific temperature for approximately 20 minutes. The measurements are executed by progressing from lower to higher temperatures within the range of 298 to 448 K and in the sequence from the lower to the larger diameter diodes. More details about the measurements set-up are described in Appendix B.

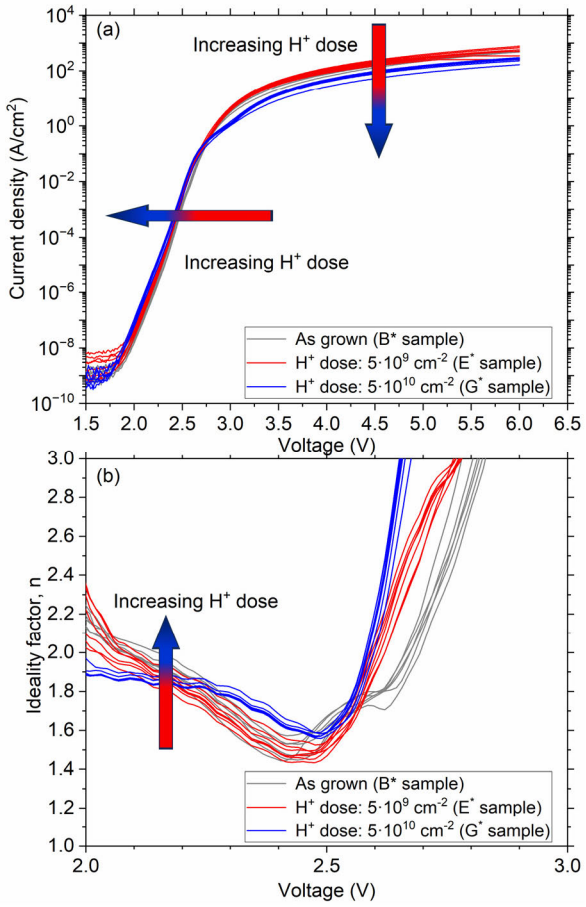

FIGURE 3. Comparison of (a) forward current density curves and (b) ideality factors of as grown packaged diodes (in grey color) and ion implanted diodes per H+ dose of 5×10^9 cm^{-2} (red color - diodes of sample E*) and 5×10^{10} cm^{-2} (blue color - diodes of samples G*).

IV. RESULTS AND DISCUSSION

A. J-V CURVES BEFORE AND AFTER H^+ IRRADITION

Analyzing the current density of non-implanted diodes across different diameters (illustrated by the grey curves in Fig. 3a), there is no evidence of increasing current density for decreasing diode diameter at a constant voltage. This observation implies the absence of any perimeter effect [15] thereby indicating the successful passivation of the mesa wall that defines the PN junction area.

The J-V curves of the 800 keV H^+ ion implanted diodes with those of the not-implanted diodes for sample B* of Table 1 are compared in Fig. 3a for the 5×10^9 cm^{-2} and the 5×10^{10}cm^{-2} doses, respectively. No significant difference is visible within the statistic spread of the J-V curves of not-implanted diodes up to an implantation dose of 5×10^9 cm^{-2} (grey and red curves in Fig. 3a almost overlap).

With increasing H^+ ion dose, the diode R_{ON} increases and the exponential trait of the J-V curve shifts towards lower

voltages showing differences with the not-implanted diodes' J-V curves that are weak but out of the statistic spread of the latter.

Blue curves in Fig. 3a show more affected devices exposed to the higher H^+ ion implantation dose of $5 \times 10^{10}cm^{-2}$.

Fig. 3b summarizes the evolution of the ideality factor curves with increasing H^+ ion dose, comparing as grown and implanted diodes for the 5×10^9 cm^{-2} and for the $5 \times 10^{10}cm^{-2}$ H^+ ion dose in the case of packaged samples. For bias voltage approximately above 2.15 V, with increasing H^+ ion dose the ideality factor curves of the implanted diodes progressively increase consistently with the rise of defect associated with the H^+ irradiation.

This voltage range corresponds to the specific trait of the current-voltage characteristic which is significantly impacted by the presence of $Z_{1/2}$ defects. This effect has been corroborated by prior simulations, as indicated in our previous work [16] and further supported in [17], where the authors demonstrated an increase in the ideality factor with rising $Z_{1/2}$ defect concentrations. The increase of ideality factor has also been noted in diodes subjected to He^+ implantation [18].

For the $Z_{1/2}$ center, an acceptor-like defect resulting from a carbon vacancy [19], has been linked to carrier lifetime reduction and identified as a detrimental defect in n-type SiC epilayers [20], [21]. Furthermore, DLTS measurements have revealed an increase in the concentration of the $Z_{1/2}$ center subsequent to proton irradiation [22], [23].

The increase in concentration of $Z_{1/2}$ with the H^+ irradiation dose, combined with the acceptor-like behavior of the defect that compensates the epitaxial layer's doping, provides an explanation for the observed shifts in the experimental J-V curves and the associated increment in R_{ON}, as illustrated in Fig. 3.

B. C-V AND N_D EXTRACTION BEFORE H^+ IRRADIATION

C-V measurements were conducted on various samples to assess the doping profile of the epilayer, and starting from that, to characterize the radiation damage resulting from H^+ implantation, with the goal of establishing a correlation with the lifetimes measured using OCVD.

Indeed, from the depletion capacitance per unit area C_A of a PN junction with uniform doping profiles and if the hypothesis of strongly asymmetric junction holds, i.e., $N_A \gg N_D$, as for diodes in this study, it is possible to extract the doping profile of the less doped side of the junction as [24]:

$$N_D = \frac{2}{\varepsilon_{SiC} q A^2} \left[\frac{d\left(1/C_A^2\right)}{dV} \right]^{-1} \tag{1}$$

where ε_{SiC} is the electrical permittivity of the semiconductor, q the electron charge, A the PN junction area, and C_A the depletion capacitance per unit area.

Due to the mesa structure deviating from the typical planar junction device (as shown in Fig. 1), our main aim was to assess whether equation (1) remained applicable for interpreting the C-V measurements.

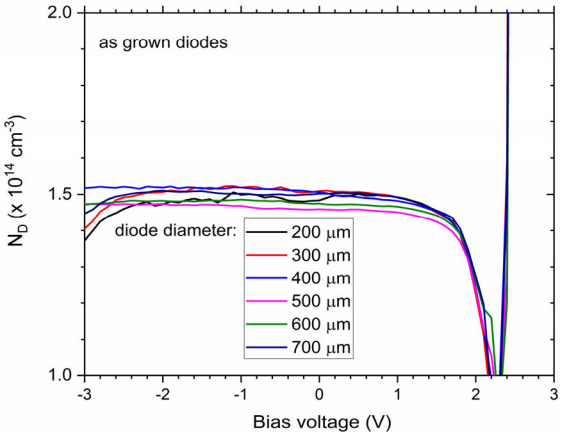

FIGURE 4. Doping profile in the epilayer, $N_D(V)$, versus the bias voltage deduced from the $C_A(V)$ by (3), in diodes of varying dimensions in their as grown state.

Unfortunately, upon analyzing the capacitance-to-area ratio derived from measurements taken on non-implanted diodes of different diameters, we observed varying values. This was unexpected, as the ratio should ideally remain constant, given its dependence solely on physical parameters that remain consistent across diodes, differing only in their respective diameters.

We thus derived the depletion capacitance component that solely depend on the PN junction radius via C-V measurements on diodes of different sizes as described in [25]: dividing the measured capacitance C by the junction area of each diode, $A = \pi \cdot r^2$, as defined in (2), enables the extraction of the area-dependent capacitance component, C_A, which represents the capacitance solely dependent on the PN junction area, excluding contributions arising from the mesa. Specifically, (2) yields $C_A = \alpha$, while terms β and γ correlate with the device's geometric characteristics [25].

$$C(V)/A = \alpha(V) + \frac{\beta(V)}{r} + \frac{\gamma(V)}{r^2} \tag{2}$$

This method enables the determination of C_A as per (3):

$$C_A(V) = \frac{C(V)}{\pi \cdot r^2} - \frac{\beta(V)}{r} - \frac{\gamma(V)}{r^2} \tag{3}$$

The doping profile $N_D(V)$, which describes the distribution of dopant concentration with respect to voltage, was determined based on (1) using values of $C_A(V)$ calculated by (3): Fig. 4 illustrates the doping profile $N_D(V)$ for diodes of varying dimensions.

For all diode diameters, the calculated doping level remains relatively uniform over a wide range of voltages, and do not show appreciable difference among different diode diameters. The calculated doping concentration in the epilayer is quite close to $N_D = 1.5 \cdot 10^{14}$ cm^{-3}, with a maximum absolute error of $\approx 3\%$ among different diodes.

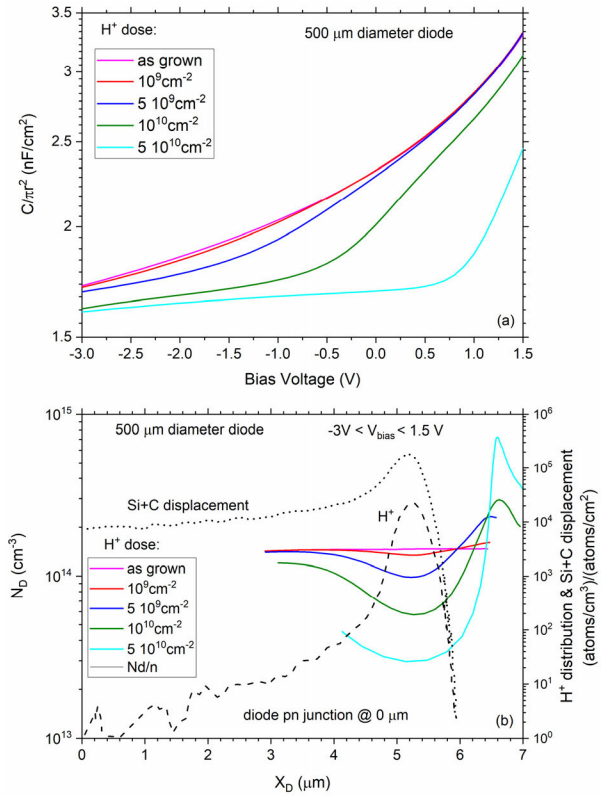

FIGURE 5. (a) Capacitance per unit area, $C_A(V)$, versus bias voltage calculated by (3); (b) left axis: doping profile deduced from $C_A(V)$ curves in (a) versus the depletion region width; right axis: depth distributions of 800 keV H^+ ions and corresponding sum of displaced Si and C atoms normalized to the H^+ ion dose. The depth distributions are simulation outputs of SRIMS2013 with 35 eV and 20 eV displacement energy for Si and C atoms, respectively, which brings to more displaced C atoms than Si ones.

As the forward bias approaches the built-in potential (φ_{bi}), the diffusion capacitance becomes increasingly significant, making equation (1) no longer applicable.

Deriving N_D directly from the measured capacitance C, rather than C_A, would lead to different doping values for diodes on the same sample. These values would span from $1.25{\cdot}10^{15}\text{cm}^{-3}$ when measured on the largest diameter diode (700 μm) to $2.1{\cdot}10^{14}\text{cm}^{-3}$ when measured on smallest diode (200 μm). This analysis was also repeated on diodes of different irradiation conditions to evaluate the possible effect of H^+ implant on the doping.

C. C-V AND N_D AFTER H^+ IRRADIATION

Fig. 5a presents the measured capacitance per unit area of a 500 μm diameter diode for different irradiation dose: it clearly shows that the capacitance behavior undergoes changes due to H^+ irradiation.

The doping profile $N_D(V)$ as a function of the depleted region, $X_D(V)$, is plotted in Fig. 5b where it is evident that H^+ implantation leads to a decrease in the N_D value. Notably, the most prominent reduction in doping is observed at a depth of around 5.5 μm from the pn junction (approximately 7 μm from the anode metal surface). This reduction is closely associated with the localized irradiation damage caused by the distribution of H^+ ions and displaced atoms in SiC, as calculated by SRIMS2013 [26](illustrated by the dashed and dotted lines in Fig. 5b). In samples implanted at room temperature it is expected that the carbon vacancy concentration is somewhat higher than the silicon vacancy concentration, assuming displacement energies of 20 (35) eV for C (Si), respectively, and with a similar dynamic annealing of $\sim$3%.

H^+ irradiation seems to reduce the concentration of free electrons by compensating for the donor doping in the epitaxial layer. This aligns with the trends seen in the experimental J-V characteristics and ideality factor discussed previously. Additionally, it correlates with the creation of defects acting as acceptors, such as the $Z_{1/2}$ defect.

The damage caused by the proton irradiation is localized just beyond the PN junction where it is effective in speeding up the diode switch-off and reducing the turn-off losses [1]: for reference, the space charge region in the not-implanted diode at 0 V and RT is 4.4 μm.

The reduced N_D is followed by a pronounced increase approximately between $x_D = 6$ and 7 μm (varying with the H^+ doses). This increase is not real and ascribed to an anomaly occurring when profiling nonuniform distributions of deep acceptor-like [27].

The impact of the implanted region on the lifetime has been investigated by measuring the lifetime of various samples using the OCVD technique, as described in the next paragraph.

D. OCVD MEASUREMENTS: τ_{HL} EXTRACTION

To accurately measure the high-level or ambipolar carrier lifetime using OCVD, it is crucial to not only ensure that the chosen bias current guarantees the diode's operation under high injection conditions, but also to confirm that the measured lifetimes are not affected by the measurement setup. The high injection regime can be validated by conducting OCVD measurements at increasing bias levels until the saturation of τ_{HL} is observed [28], [29]. Conversely, conducting measurements with various R_{EXT} values connected in parallel to the diode under test helps identify the optimal R_{EXT} value for compensating the experimental setup's impact on the measured lifetime, as detailed in [14]. τ_{HL} is computed by the formula [30]:

$$\tau_{HL} = -2 \cdot \frac{kT/q}{dV/dt} \approx \tau_n + \tau_p \tag{4}$$

where k is the Boltzmann constant, T the absolute temperature, q the electron charge, dV/dt the slope of the OCVD curve during the period of high injection operation, while τ_n and τ_p correspond to the low-level lifetimes of electrons and holes, respectively.

A bias current of 1 A is found adequate to achieve high injection levels in diodes of all sizes. Moreover, this value also avoids the occurrence of large ringing phenomena

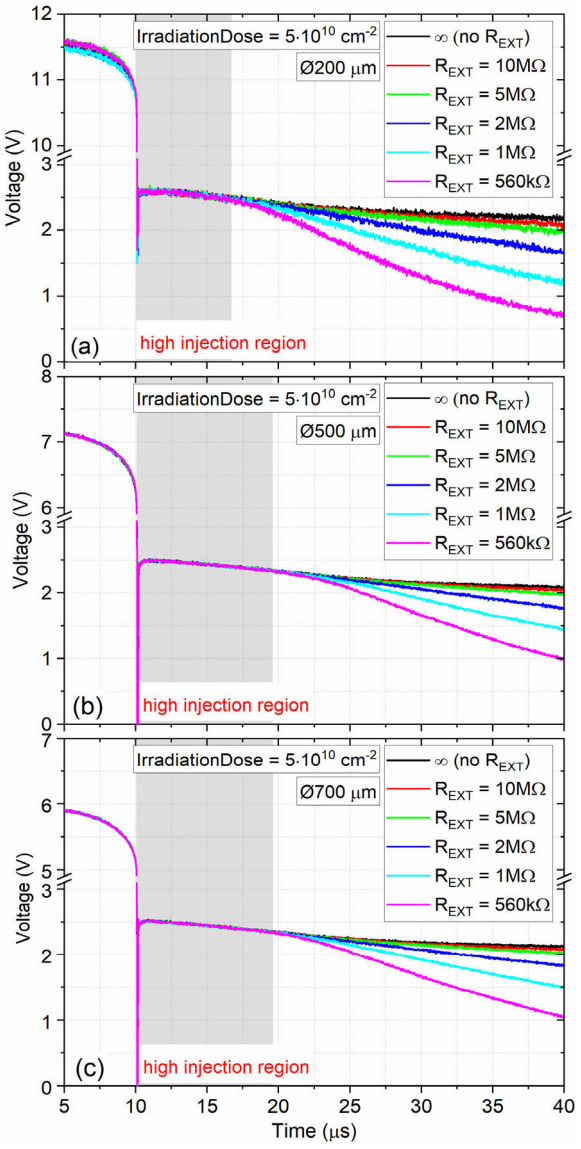

FIGURE 6. OCVD curves at 298 K of (a) 200 μm, (b) 500 μm, and (c) 700 μm diameter diodes of sample G* (5 × 10^{10} cm^{-2} H$^+$ ion implanted) for different external resistance R_{EXT}. The grey colour background highlights the decay time region corresponding to the high injection condition.

observed at higher bias current levels that limited the measurement range. Additionally, diodes with smaller diameters can accommodate a maximum of two bonding wires, thus imposing a limit on the maximum current to prevent wire burnout.

The τ_{HL} can be calculated by (4) from the slope of the linear trait of the voltage decay.

Fig. 6(a-c) illustrate the OCVD curves at a constant current bias, but with varying R_{EXT} values, for diodes of different diameters following a 5 × 10^{10}cm^{-2} H$^+$ ion irradiation dose. The OCVD measurements have been performed on all diodes, as-grown or after H$^+$ implantation, within the temperature range of 298−448 K.

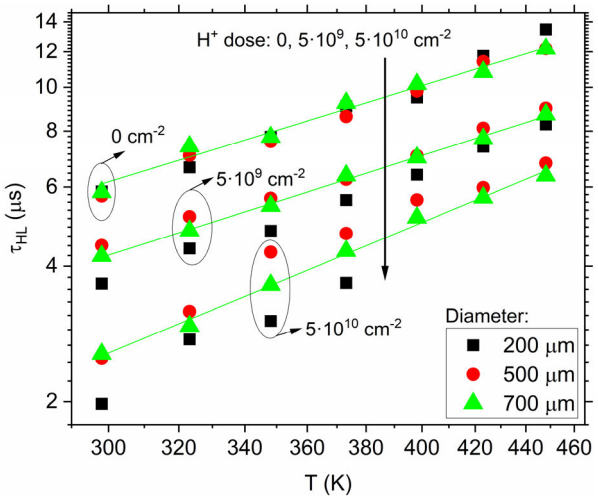

FIGURE 7. Temperature dependence of τ_{HL} for diodes with different diameters and irradiation dose in log-log scale. The solid line is generated by interpolating the data for a 700 μm diameter using the power law in (5).

E. MEASURED τ_{HL} AT DIFFERENT TEMPERATURES AND H$^+$ DOSE

Fig. 7 presents data obtained from diodes of various diameter (200−500−700 μm) and different H$^+$ irradiation dose, namely 0 (as-grown), $5{\cdot}10^9$ and $5{\cdot}10^{10}$ cm^{-2}. The OCVD-measured lifetime represents an averaged value influenced by both the carrier lifetime of the as-grown semiconductor and the decreasing lifetime due to H$^+$ implantation across a region that expands as the implantation dose increases, as depicted in Fig. 5.

The τ_{HL} curves of varying diameter diodes versus temperature almost overlap up to 400 K in the case of as grown diodes, while they feature some difference in the case of the smallest diameter diode and larger implantation dose.

The carrier lifetime in a semiconductor, τ_{TOT}, can be seen as arising from the contribution of the carrier lifetime due to recombination in the bulk of semiconductor, denoted as τ_B, and a surface lifetime, τ_s, accounting for recombination at device surfaces. The overall lifetime can be expressed as $1/\tau_{TOT} = 1/\tau_B + 1/\tau_s$ [31].

This equation is applicable to the studied case, as the behavior of the implanted region closely resembles that of a region with a reduced lifetime, possibly associated with a surface recombination velocity. Furthermore, the extension of the implanted region into the bulk introduces additional complexity as it impacts on this lifetime component too.

The relationship between the measured lifetime and the diode geometry is not easy to obtain; however, a dependence of $1/\tau_s$ on 1/r or $1/r^2$, with r being the PN junction radius, has been calculated for simple geometries in the limits of low and high surface recombination velocity, [31], [32], respectively, and for constant τ_B. This can help explain the observed dependence of measured lifetime on diode dimension and dose. We thus focus our analysis to τ_{HL} data of the 700 μm diode, where the contribution of $1/\tau_s$ is lowest.

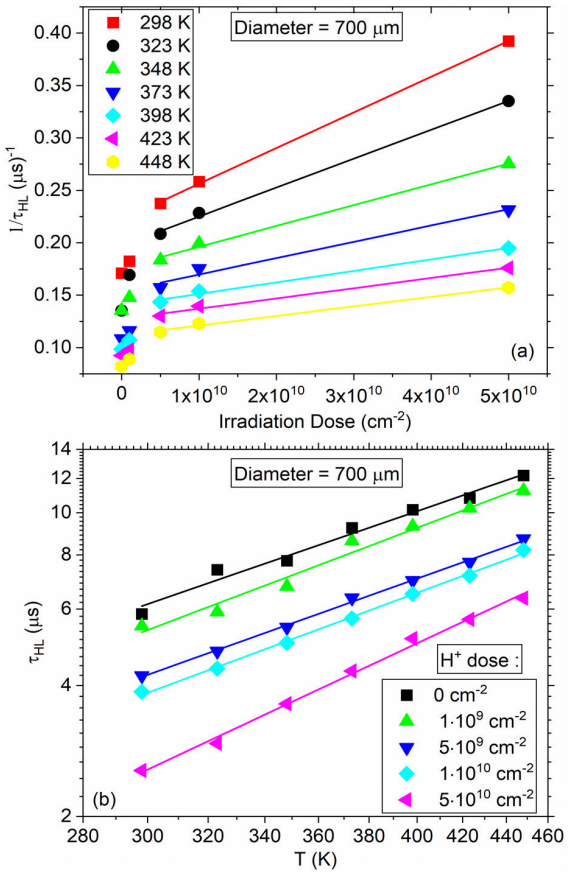

FIGURE 8. (a) $1/\tau_{HL}$ measured on the 700 μm diode versus the H^+ ion dose at a given temperature of measurement (symbols); solid lines are generated by linear interpolating the measured $1/\tau_{HL}$; (b) τ_{HL} versus the measurement temperature for given H^+ ion dose in a log-log scale (symbols); solid lines are generated by interpolating the measured τ_{HL}.

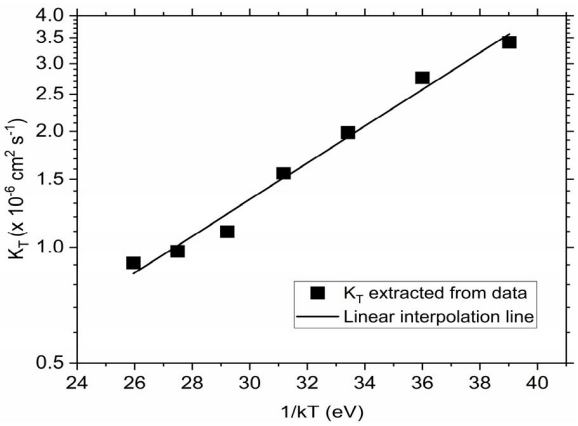

FIGURE 9. Arrhenius plot of the damage coefficient, K_T, derived from $1/\tau_{HL}$ data in Fig. 8a for irradiated diodes of 700 μm diameter.

At 300 K, for the un-implanted diode with a diameter of 700 μm, an average carrier density of $\sim 4 \times 10^{17}$ cm^3 has been calculated in the epilayer using equation reported in [1]. This carrier density is below the value at which Auger recombination becomes significant [33].

Figs. 8(a,b) show the τ_{HL} values of 700 μm diodes after H^+ ion implantation at different doses in the range $1 \times 10^9 - 5 \times 10^{10}$ cm^{-2} and for different temperatures of measurement in the range 298 – 448 K.

Upon examining the curves, τ_{HL} decreases with an increase in ion dose and rises with an increase in the measurement temperature. Additionally, at the highest implantation dose, there is a rise in the slope of the log-log curve depicting τ_{HL} versus temperature (Fig. 8b).

F. ESTIMATION OF DAMAGE COEFFICIENT

In prior studies involving Silicon [34] and SiC [23], a direct correlation was established between the inverse of the carrier lifetime and the implanted dose.

This correlation was quantified by a coefficient known as the damage coefficient, K_T, that is related with the quantity of induced defects and is contingent upon both the energy of ions employed to induce damage and the type of particle utilized in the process.

In Fig. 8a, except for the point representing the lowest fluence, a clear linear relationship emerges between $1/\tau_{HL}$ and irradiation doses, particularly noticeable for higher H^+ doses, ϕ. The slope of this line represents the damage coefficient, K_T [35]. At T=293 K the derived damage coefficient from the dataset in Fig.8a is $3.4 \cdot 10^{-6}$ cm^2 s^{-1}.

We observed that K_T decreases with the rise in measurement temperature, demonstrating an Arrhenius-type temperature dependency, as depicted in Fig. 9. The resulting Arrhenius plot reveals an activation energy of 48 meV.

G. TEMPERATURE-DRIVEN POWER LAW FOR τ_{HL}

We conducted an analysis of the τ_{HL} temperature dependence at a constant H^+ ion dose.

Curves of Fig. 8(b) were fitted by an empirical power law [36], as usually done in silicon device, given in (5):

$$\tau = \tau_0 \left(\frac{T}{T_0} \right)^{\alpha} \tag{5}$$

where τ_0 is the lifetime value at the temperature $T_0 = 298$ K and α the power law exponent obtained by fitting the experimental curves.

Specifically, from the data analysis, it was observed that the interpolation of the measured lifetimes in the larger diameter diodes is consistently characterized by an R-square value greater than 0.99.

Table 2 gives the estimated α exponent for $T_0 = 298$ K on not implanted and H^+ implanted 700 μm diameter diode and the corresponding τ_0 obtained from OCVD measured τ_{HL}.

Previous studies on as-grown diodes have reported the same exponential law dependence on temperature with values of α as 1.5 [10], 1.72 [37], 1.84 [11], 1.9 [38]. Table 2 's results indicate a noticeable trend: the temperature dependence of τ_{HL} appears to intensify with the highest H^+ ion dose. This observed trend suggests a threshold-like behavior on the irradiation dose in the τ_{HL} temperature dependence.

TABLE 2. α and T_0 obtained from the fitting of experimental data with (5) per diodes of 700 μm diameter; as grown and H^+ implanted samples.

H^+ dose (ATOMS/CM^2)	α	τ_0 (μs)
0	1.7	6.09
10^9	1.9	5.30
$5{\cdot}10^9$	1.8	4.18
10^9	1.8	3.80
$5{\cdot}10^{10}$	2.3	2.52

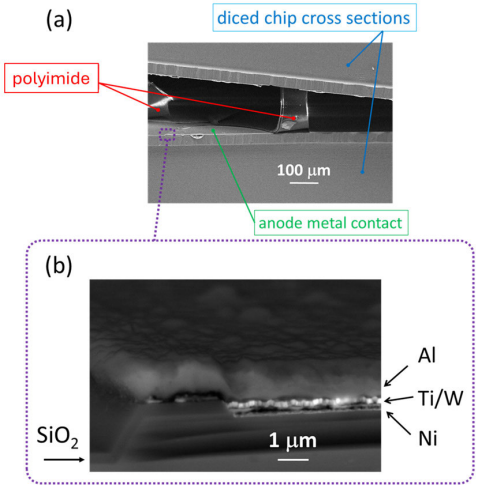

FIGURE 10. (a) SEM image of the cross sections of a cleaved sample chip; the two parts of the sample are flipped one faced to the other because linked together by a polyimide film that protects the sample surface. The anode contact of a cross-sectioned diode is visible at the surface of the bottom pieces of the sample. (b) Enlarged view of the diode perimeter cross section. Mesa etchings profiles, surface passivation layer (SiO2), and multilayers structure of the anode contact are visible. Identification of the metals in the multilayers anode contact is by electron dispersive spectroscopy (EDS) microanalysis.

V. CONCLUSION

We examined the variations in carrier lifetime with temperature in Silicon Carbide (SiC) diodes exposed to H^+ irradiation within a dose range of 10^9 to $5{\cdot}10^{10}$ cm^{-2}. The goal was to identify an empirical law suitable for TCAD modelling of SiC devices, capable of accurately describing the evolution of carrier lifetime with temperature and potential alterations arising from proton irradiation.

Through the electrical characterization of diodes of various diameters subjected to different H^+ irradiation doses, we observed variations in current-voltage and ideality factor curves as the irradiation dose increases, which resulted in elevated on resistance (R_{ON}), decreased built-in voltage, and increased ideality factor, that we attributed to an increase in acceptor-type defects ($Z_{1/2}$) generated during irradiation, in agreement with previous studies.

The estimation of epilayer doping through C-V measurements for various irradiation doses revealed a gradual reduction in layer doping as the H^+ dose increases, consistent with the acceptor nature of the $Z_{1/2}$ defect induced by H^+ irradiation.

The doping reduction has a spatial distribution closely correlated with the depth distributions of 800 keV H^+ ions and displaced atoms simulated using SRIMS2013, and it is localized just beyond the PN junction. In this location, it is effective in shortening the diode switch-off and reducing turn-off losses.

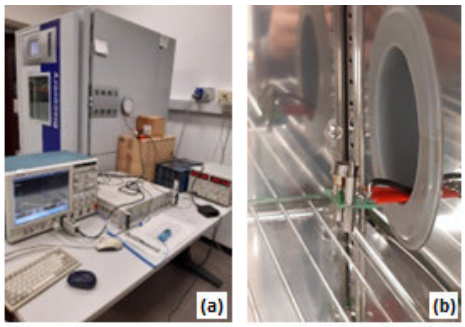

FIGURE 11. Experimental setup used for OCVD measurements: (a) test bench; (b) the TO-8 case inside the climatic chamber.

High injection carrier lifetime was measured using OCVD technique conducted at different temperatures in the range from 298 to 448 K on both as grown and irradiated diodes.

Excluding the point corresponding to the lowest irradiation dose, the analysis indicated a proportional law between the inverse of the lifetime and the irradiation dose. The proportionality factor, also known as the damage coefficient (K_T), exhibited an Arrhenius dependence on temperature.

The OCVD measured carrier lifetime shows a decrease with an increasing ion dose and an increase with rising measurement temperature. The temperature dependence of the lifetime follows a power-law relationship across all irradiation doses, with the exponent becoming higher at the highest H^+ ion dose.

APPENDIX A
SEM ANALYSYS

The depth structure and composition of the device cross section as obtained by SEM analyses of a cross sectioned specimen are shown in Fig.10. The hypothesized scheme of the half cross-section of the vertical PiN diode around the central axis of symmetry depicted in Fig.1, the doping signs and concentrations values of the homo-epitaxial and bulk layers come Fig.10 and the SiC wafer data sheet.

APPENDIX B
OCVD SETUP

We utilized a TTi QL355TP power supply for diode biasing, which is isolated from the device through a Pickering mercury wetted switch relay, with a maximum operating current of 3 A and an open-circuit resistance greater than 10^{12} MΩ [39]. The relay is under the control of a Philips PM5781 programmable pulse generator, enabling precise on/off switching. Finally, a Tektronix P6139A passive probes alongside a Tektronix TCP0030, connected to an 8-bit Tektronix DPO7254 Digital oscilloscope with a sampling rate of up to 20 GSa/s, are used to probe the voltage and current waveforms. Fig. 11 displays the test-bench used in OCVD measurements.

ACKNOWLEDGMENT

The authors acknowledge the contribution of Dr. Virginia Boldrini who wire bonded the samples on the TO-8 cases and that of Franco Corticelli who performed the SEM observations.

REFERENCES

[1] B. J. Baliga, *Fundamentals of Power Semiconductor Devices*. Boston, MA, USA: Springer, 2010, doi: 10.1007/978-0-387-47314-7.
[2] G. Iannaccone, C. Sbrana, I. Morelli, and S. Strangio, "Power electronics based on wide-bandgap semiconductors: Opportunities and challenges," *IEEE Access*, vol. 9, pp. 139446–139456, 2021, doi: 10.1109/ACCESS.2021.3118897.
[3] L. Han, L. Liang, Y. Kang, and Y. Qiu, "A review of SiC IGBT: Models, fabrications, characteristics, and applications," *IEEE Trans. Power Electron.*, vol. 36, no. 2, pp. 2080–2093, Feb. 2021, doi: 10.1109/TPEL.2020.3005940.
[4] T. Kimoto, H. Niwa, T. Okuda, E. Saito, Y. Zhao, S. Asada, and J. Suda, "Carrier lifetime and breakdown phenomena in SiC power device material," *J. Phys. D, Appl. Phys.*, vol. 51, no. 36, Sep. 2018, Art. no. 363001, doi: 10.1088/1361-6463/aad26a.
[5] T. Kimoto and H. Watanabe, "Defect engineering in SiC technology for high-voltage power devices," *Appl. Phys. Exp.*, vol. 13, no. 12, Dec. 2020, Art. no. 120101, doi: 10.35848/1882-0786/abc787.
[6] P. Dong, Y. Qin, X. Yu, X. Xu, Z. Chen, L. Li, and Y. Cui, "Electron radiation effects on the 4H-SiC PiN diodes characteristics: An insight from point defects to electrical degradation," *IEEE Access*, vol. 7, pp. 170385–170391, 2019, doi: 10.1109/ACCESS.2019.2955385.
[7] P. Hazdra and S. Popelka, "Lifetime control in SiC PiN diodes using radiation defects," *Mater. Sci. Forum*, vol. 897, pp. 463–466, May 2017, doi: 10.4028/www.scientific.net/msf.897.463.
[8] P. Hazdra, S. Popelka, and A. Schöner, "Local lifetime control in 4H-SiC by proton irradiation," *Mater. Sci. Forum*, vol. 924, pp. 436–439, Jun. 2018, doi: 10.4028/www.scientific.net/msf.924.436.
[9] P. Hazdra, S. Popelka, and A. Schöner, "Optimization of SiC power p-i-n diode parameters by proton irradiation," *IEEE Trans. Electron Devices*, vol. 65, no. 10, pp. 4483–4489, Oct. 2018, doi: 10.1109/TED.2018.2866763.
[10] S. Sapienza, G. Sozzi, D. Santoro, P. Cova, N. Delmonte, G. Verrini, and G. Chiorboli, "Correlation between OCVD carrier lifetime vs temperature measurements and reverse recovery behavior of the body diode of SiC power MOSFETs," *Microelectron. Rel.*, vol. 113, Oct. 2020, Art. no. 113937, doi: 10.1016/j.microrel.2020.113937.
[11] K. Tian, J. Xia, K. Elgammal, A. Schöner, W. Kaplan, R. Karhu, J. Ul-Hassan, and A. Hallén, "Modelling the static on-state current voltage characteristics for a 10 kV 4H–SiC PiN diode," *Mater. Sci. Semicond. Process.*, vol. 115, Aug. 2020, Art. no. 105097, doi: 10.1016/j.mssp.2020.105097.
[12] *UiO MiNaLab is One of Four Cleanroom Facilities Within the Norwegian National Infrastructure, The Norwegian Micro and Nanofabrication Facility, NorFab*. Accessed: Apr. 17, 2024. [Online]. Available: https://www.mn.uio.no/fysikk/english/research/about/infrastructure/facilities/material-characterisation/micro-nano/norfab/
[13] M. A. Green, "Minority carrier lifetimes using compensated differental open circuit voltage decay," *Solid-State Electron.*, vol. 26, no. 11, pp. 1117–1122, Nov. 1983, doi: 10.1016/0038-1101(83)90011-4.
[14] G. Sozzi, S. Sapienza, R. Nipoti, and G. Chiorboli, "OCVD measurement of ambipolar and minority carrier lifetime in 4H-SiC devices: Relevance of the measurement setup," *IEEE Trans. Electron Devices*, vol. 68, no. 7, pp. 3254–3260, Jul. 2021, doi: 10.1109/TED.2021.3083211.
[15] R. Nipoti, M. Puzzanghera, G. Sozzi, and R. Menozzi, "Perimeter and area components in the I–V curves of 4H-SiC vertical p^+-i-n diode with Al^+ ion-implanted emitters," *IEEE Trans. Electron Devices*, vol. 65, no. 2, pp. 629–635, Feb. 2018, doi: 10.1109/TED.2017.2779602.
[16] G. Sozzi, M. Puzzanghera, R. Menozzi, and R. Nipoti, "The role of defects on forward current in 4H-SiC p-i-n diodes," *IEEE Trans. Electron Devices*, vol. 66, no. 7, pp. 3028–3033, Jul. 2019, doi: 10.1109/TED.2019.2917534.
[17] M. L. Megherbi, F. Pezzimenti, L. Dehimi, A. Saadoune, and F. G. Della Corte, "Analysis of the forward I–V characteristics of Al-implanted 4H-SiC p-i-n diodes with modeling of recombination and trapping effects due to intrinsic and doping-induced defect states," *J. Electron. Mater.*, vol. 47, no. 2, pp. 1414–1420, Feb. 2018, doi: 10.1007/s11664-017-5916-8.
[18] D. Pellegrino, L. Calcagno, M. Zimbone, S. Di Franco, and A. Sciuto, "Correlation between defects and electrical performances of ion-irradiated 4H-SiC p–n junctions," *Materials*, vol. 14, no. 8, p. 1966, Apr. 2021, doi: 10.3390/ma14081966.
[19] N. T. Son, X. T. Trinh, L. S. Løvlie, B. G. Svensson, K. Kawahara, J. Suda, T. Kimoto, T. Umeda, J. Isoya, T. Makino, T. Ohshima, and E. Janzén, "Negative-U system of carbon vacancy in 4H-SiC," *Phys. Rev. Lett.*, vol. 109, no. 18, Oct. 2012, Art. no. 187603, doi: 10.1103/physrevlett.109.187603.
[20] R. Nipoti, M. Puzzanghera, and G. Sozzi, "Al^+ ion implanted 4H-SiC vertical p^+-i-n diodes: Processing dependence of leakage currents and OCVD carrier lifetimes," *Mater. Sci. Forum*, vol. 897, pp. 439–442, May 2017, doi: 10.4028/www.scientific.net/msf.897.439.
[21] P. B. Klein, "Identification and carrier dynamics of the dominant lifetime limiting defect in n^-4H-SiC epitaxial layers," *Phys. Status Solidi (A)*, vol. 206, no. 10, pp. 2257–2272, Oct. 2009, doi: 10.1002/pssa.200925155.
[22] G. Alfieri, A. Mihaila, R. Nipoti, M. Puzzanghera, G. Sozzi, P. Godignon, and J. Millán, "Point defects investigation of high energy proton irradiated SiC p^+-i-n diodes," *Mater. Sci. Forum*, vol. 897, pp. 246–249, May 2017, doi: 10.4028/www.scientific.net/msf.897.246.
[23] P. Hazdra and S. Popelka, "Displacement damage and total ionisation dose effects on 4H-SiC power devices," *IET Power Electron.*, vol. 12, no. 15, pp. 3910–3918, Dec. 2019, doi: 10.1049/iet-pel.2019.0049.
[24] S. M. Sze, *Physics of Semiconductor Devices*, 3rd ed. Hoboken, NJ, USA: Wiley, 2007.
[25] G. Sozzi, G. Chiorboli, L. Perini, and R. Nipoti, "Investigating mesa structure impact on C-V measurements," *IEEE Access*, vol. 12, pp. 32938–32943, 2024, doi: 10.1109/access.2024.3366090.
[26] J. F. Ziegler. *SRIM2013 Code Download*. Accessed: Apr. 17, 2024. [Online]. Available: http://www.srim.org/index.htm
[27] L. C. Kimerling, "Influence of deep traps on the measurement of free-carrier distributions in semiconductors by junction capacitance techniques," *J. Appl. Phys.*, vol. 45, no. 4, pp. 1839–1845, Apr. 1974, doi: 10.1063/1.1663500.
[28] D. K. Schroder and L. G. Rubin, "Semiconductor material and device characterization," *Phys. Today*, vol. 44, no. 4, pp. 107–108, Apr. 1991, doi: 10.1063/1.2810086.
[29] G. Sozzi, M. Puzzanghera, G. Chiorboli, and R. Nipoti, "OCVD lifetime measurements on 4H-SiC bipolar planar diodes: Dependences on carrier injection and diode area," *IEEE Trans. Electron Devices*, vol. 64, no. 6, pp. 2572–2578, Jun. 2017, doi: 10.1109/TED.2017.2691280.
[30] H. Schlangenotto and W. Gerlach, "On the post-injection voltage decay of p-s-n rectifiers at high injection levels," *Solid-State Electron.*, vol. 15, no. 4, pp. 393–402, Apr. 1972.
[31] W. Schockley, *Electrons and Holes in Semiconductors*. New York, NY, USA: D. Van Nostrand Company, 1950.
[32] D. T. Stevenson and R. J. Keyes, "Measurement of carrier lifetimes in germanium and silicon," *J. Appl. Phys.*, vol. 26, no. 2, pp. 190–195, Feb. 1955, doi: 10.1063/1.1721958.
[33] A. Galeckas, J. Linnros, V. Grivickas, U. Lindefelt, and C. Hallin, "Auger recombination in 4H-SiC: Unusual temperature behavior," *Appl. Phys. Lett.*, vol. 71, no. 22, pp. 3269–3271, Dec. 1997, doi: 10.1063/1.120309.
[34] J. Vanhellemont, E. Simoen, C. Claeys, A. Kaniava, E. Gaubas, G. Bosman, B. Johlander, L. Adams, and P. Clauws, "On the impact of low fluence irradiation with MeV particles on silicon diode characteristics and related material properties," *IEEE Trans. Nucl. Sci.*, vol. 41, no. 6, pp. 1924–1931, Dec. 1994, doi: 10.1109/23.340525.
[35] A. L. Barry, B. Lehmann, D. Fritsch, and D. Braunig, "Energy dependence of electron damage and displacement threshold energy in 6H silicon carbide," *IEEE Trans. Nuclear Sci.*, vol. 38, no. 6, pp. 1111–1115, Dec. 1991, doi: 10.1109/23.124082.
[36] S. Rein, "Material science," in *Lifetime Spectroscopy: A Method of Defect Characterization in Silicon for Photovoltaic Applications*. Berlin, Germany: Springer, 2006.
[37] B. Buono, R. Ghandi, M. Domeij, B. G. Malm, C.-M. Zetterling, and M. Ostling, "Modeling and characterization of current gain versus temperature in 4H-SiC power BJTs," *IEEE Trans. Electron Devices*, vol. 57, no. 3, pp. 704–711, Mar. 2010, doi: 10.1109/TED.2009.2039099.
[38] A. Udal and E. Velmre, "Investigation of charge carrier lifetime temperature-dependence in 4H-SiC diodes," *Mater. Sci. Forum*, vols. 556–557, pp. 375–378, Sep. 2007, doi: 10.4028/www.scientific.net/msf.556-557.375.
[39] *Pickering Electronics*. Accessed: Apr. 17, 2024. [Online]. Available: http://www.pickeringrelay.com/

Open Access funding provided by 'Università degli Studi di Parma' within the CRUI CARE Agreement